Thin Solid Films xxx (2014) xxx–xxx

Contents lists available at ScienceDirect

Thin Solid Films

journal homepage: www.elsevier.com/locate/tsf

Optical Mueller matrix modeling of chiral $Al_xIn_{1-x}N$ nanospirals

Roger Magnusson *, Jens Birch, Per Sandström, Ching-Lien Hsiao, Hans Arwin, Kenneth Järrendahl

Department of Physics, Chemistry and Biology, Linköping University, SE 581 83 Linköping, Sweden

ARTICLE INFO

Available online xxxx

Keywords:
Chiral nanostructures
Mueller matrix spectroscopic ellipsometry
Anisotropy
Optical modeling
High degree of circular polarization

ABSTRACT

Metamaterials in the form of chiral nanostructures have shown great potential for applications such as chemical and biochemical sensors and broadband or wavelength tunable circular polarizers. Here we demonstrate a method to produce tailored transparent chiral nanostructures with the wide-bandgap semiconductor $Al_xIn_{1-x}N$. A series of anisotropic and transparent films of $Al_xIn_{1-x}N$ were produced using curved-lattice epitaxial growth on metallic buffer layers. By controlling the sample orientation during dual magnetron sputter deposition, nanospirals with right-handed or left-handed chirality were produced. Using a dual rotating compensator ellipsometer in reflection mode, the full Mueller matrix was measured in the spectral range 245–1700 nm at multiple angles of incidence. The samples were rotated one full turn around their normal during measurements to provide a complete description of the polarization properties in all directions. For certain wavelengths, unpolarized light reflected off these films becomes highly polarized with a polarization state close to circular. Nanostructured films with right- and left-handed chirality produce reflections with right- and left-handed near-circularly polarized light, respectively. A model with a biaxial layer in which the optical axes are rotated from bottom to top was fitted to the Mueller-matrix data. Hence we can perform non-destructive structural analysis of the complex thin layers and confirm the tailored structure. In addition, the refractive index, modeled with a biaxial Cauchy dispersion model, is obtained for the $Al_xIn_{1-x}N$ films.

© 2014 The Authors. Published by Elsevier B.V. This is an open access article under the CC BY-NC-ND license (http://creativecommons.org/licenses/by-nc-nd/3.0/).

1. Introduction

Circular polarizers made from e.g. nanostructured materials exhibiting chirality [1,2] or cholesteric liquid crystals [3] have uses in many areas, for instance in optical communication and as tunable filters [4]. Here we introduce a method of making chiral reflectors of $Al_xIn_{1-x}N$ nanostructures grown by curved-lattice epitaxial growth (CLEG) using magnetron sputtering [5]. This growth mechanism has been shown to produce a stress-free single crystal material in the form of curved rods on the nano-scale [5–7]. The curving of these nanorods occurs due to a graded lattice constant which is the result of a lateral composition gradient achieved by a spatial separation of the directional flux of material from the Al and In targets [6]. If the sample is rotated during growth the reorientation of the curved nanorods will result in a spiral shaping of the rods, hereafter referred to as nanospirals. Thus, the formed nanorods will exhibit an external chirality. The spiral shape is seen in Fig. 1. In addition, and most important for this study, the rotated compositionally graded crystal planes within the rods will result in an internal chirality.

The semiconductor $Al_xIn_{1-x}N$ has a wide and tunable bandgap which makes it suitable for transparent optical elements. It also has high thermal stability and high breakdown voltage which gives it a wider application range than e.g. liquid crystals. The nanostructured material described above is therefore in many aspects unique making structural and optical characterizations very interesting.

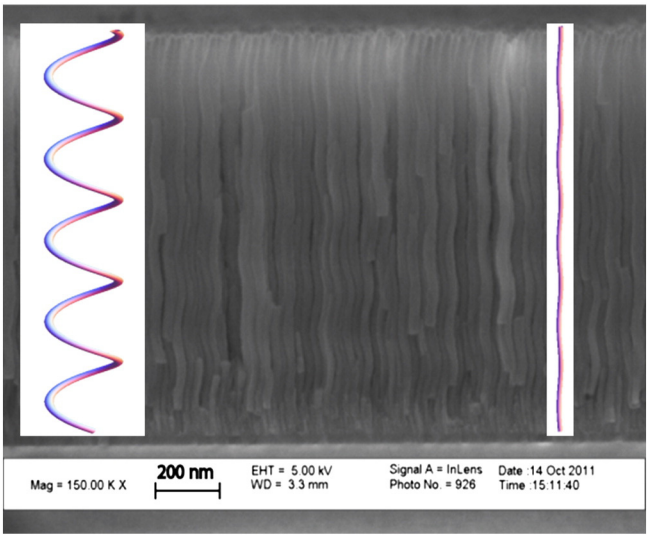
Our objectives in this work have been to i) fabricate $Al_xIn_{1-x}N$ chiral nanostructures reflecting light with a very high degree of circular polarization; ii) measure the polarizing properties of the anisotropic structures using Mueller matrix spectroscopic ellipsometry (MMSE); and iii) model the MMSE data using a multilayer model to extract structural and optical properties.

2. Theory and calculations

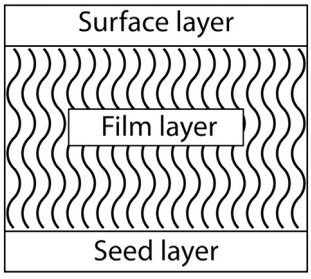
In many cases the first column of the Mueller matrix is of special interest, as it shows the same data as would be seen in the Stokes vector of the reflected light if the sample was illuminated with unpolarized light [8]. Thus, the Stokes vector $\mathbf{S} = (I, Q, U, V)^T$ (T indicates transpose) of light specularly reflected off the sample under this illumination can be extracted from the Mueller matrix by simply copying the first column of the matrix. From the Stokes vector, the degree of circular polarization P_c, can be determined by

* Corresponding author. Tel.: +46 13 282650; fax: +46 13 137568.
E-mail address: rogma@ifm.liu.se (R. Magnusson).

http://dx.doi.org/10.1016/j.tsf.2014.02.015
0040-6090 /© 2014 The Authors. Published by Elsevier B.V. This is an open access article under the CC BY-NC-ND license (http://creativecommons.org/licenses/by-nc-nd/3.0/).



the parameter V as $P_c = V / I$. In this work the general Mueller matrix elements (M_{ij}) are normalized according to $m_{ij} = \frac{M_{ij}}{M_{11}}$, giving a normalized Mueller matrix (m_{ij}) with $m_{11} = 1$. With normalized Stokes vectors ($I = 1$) the degree of circular polarization will therefore be the same as that of the m_{41} element, i.e. $P_c = V = m_{41}$. The optical properties of the investigated nanostructures become rather complicated. First, the columnar structure will have different refractive indices parallel and perpendicular to the nanorods due to form birefringence as a result of screening effects [9]. Furthermore, there is an intrinsic anisotropy since the hexagonal wurtzite crystal structure is oriented with its a-axis perpendicular and the c-axis parallel to the columns. These two anisotropies could, approximately, be modeled with a uniaxial model. In addition, however, the lateral composition gradient will give different properties in the directions parallel and perpendicular to the gradient. When all these effects are taken into account three different refractive indices in three orthogonal directions are required to describe the optical properties of the material, i.e. it needs to be biaxial. To analyze the optical data we have used a model, schematically shown in Fig. 2, with a twisted biaxial layered film representing the nanostructured $Al_xIn_{1-x}N$ film on top of an isotropic seed layer representing opaque TiN as described below.



The chiral structure of the nanorod film is modeled by a linear rotation of the direction of the two orthogonal optical axes, x and y, i.e. a Euler rotation φ around the z-axis. Surface roughness and tapering at the top of the nanocolumns, as can be observed in Fig. 1, are modeled with a biaxial Bruggeman EMA surface layer [10] using the same refractive index as in the biaxial layer mixed with 50% void. The biaxial layer optical properties are modeled with refractive indices according to two-term Cauchy dispersions $n = A/\lambda^2 + B/\lambda^4$ and extinction coefficients according to Urbach absorption tails $k = A_k e^{B_k/\lambda}$ [10] for each of the three directions, x, y and z. The layer representing the nanostructured film is divided into 100 sublayers, each with three different refractive indices along three orthogonal directions as shown in Fig. 3a. The directions of the two optical axes in the xy-plane of the sublayer closest to the substrate, are determined by the starting angle for the x-axis, φ_0. The Euler angle, φ, of each sublayer is then determined by a linear equation, $\varphi = \varphi_0 + T \cdot 360 \cdot P$, where P is a parameter identifying the sublayer and varies in steps of 0.01 from zero at the bottom of the film layer (first sublayer) to one at the top of the film layer (last sublayer). The fit parameter T then shows directly how many turns the nanospirals in the film undergo from bottom to top. The orientation of the x-axis will rotate linearly from bottom to top of the graded layer, as seen in Fig. 3b and c.

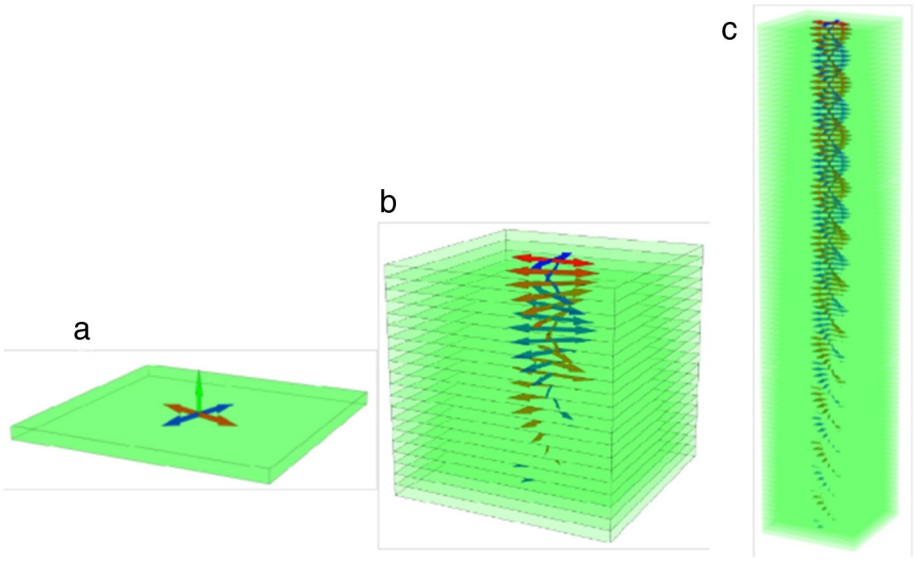
3. Experimental details

The $Al_xIn_{1-x}N$ nanostructures were grown by ultra-high vacuum magnetron sputter epitaxy on c-plane sapphire substrates with a 200 nm TiN seed layer. Since the samples were co-sputtered by one Al and one In targets with an oblique angle of ~30° towards the center from different directions, the nucleation starts on the surface with a higher InN mole fraction on one side of each nanorod and a higher AlN mole fraction at the other side. As schematically demonstrated in Fig. 4, each atomic layer thus will get a compositional gradient which depends on the orientation of the layer in the deposition chamber during deposition. As the deposition continues, self-shadowing and low surface mobility will continue the separation of InN and AlN giving each atomic layer within a rod the same compositional gradient and making the rods curved towards the more AlN-rich side [6]. By control of the substrate rotation with respect to the orientation of the deposition fluxes, left- and right-handed nanospirals were obtained. The substrate rotation speed was adjusted to the deposition rate to yield a 200 nm pitch with a 360° rotation. This deposition scheme resulted in nanospirals showing chirality not only due to the external morphology but also due to the internal crystalline structure as discussed above. Samples were manufactured with the substrate rotated five complete turns during the growth.

The samples were measured using Mueller matrix spectroscopic ellipsometry (MMSE) in the spectral range 245–1700 nm at incidence angles from 25° to 65° in steps of 10°. Each sample was rotated 360° during measurement and 72 Mueller matrices were collected, one for every 5° rotation. The instrument used was an RC2™ from J.A. Woollam Co., Inc. and analysis were performed with the software CompleteEASE™, also from J.A. Woollam Co., Inc. The ellipsometer is a dual rotating compensator instrument and all elements m_{ij} ($i, j = 1, 2, 3, 4$) of the normalized Mueller matrix are obtained. The scanning electron micrographs were taken using a LEO-1550 FE-SEM.

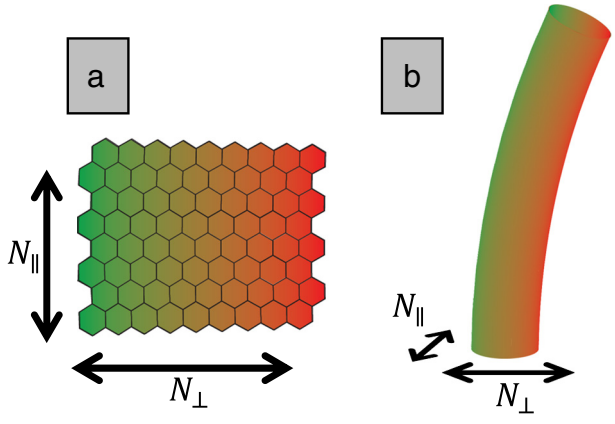
4. Results and discussion

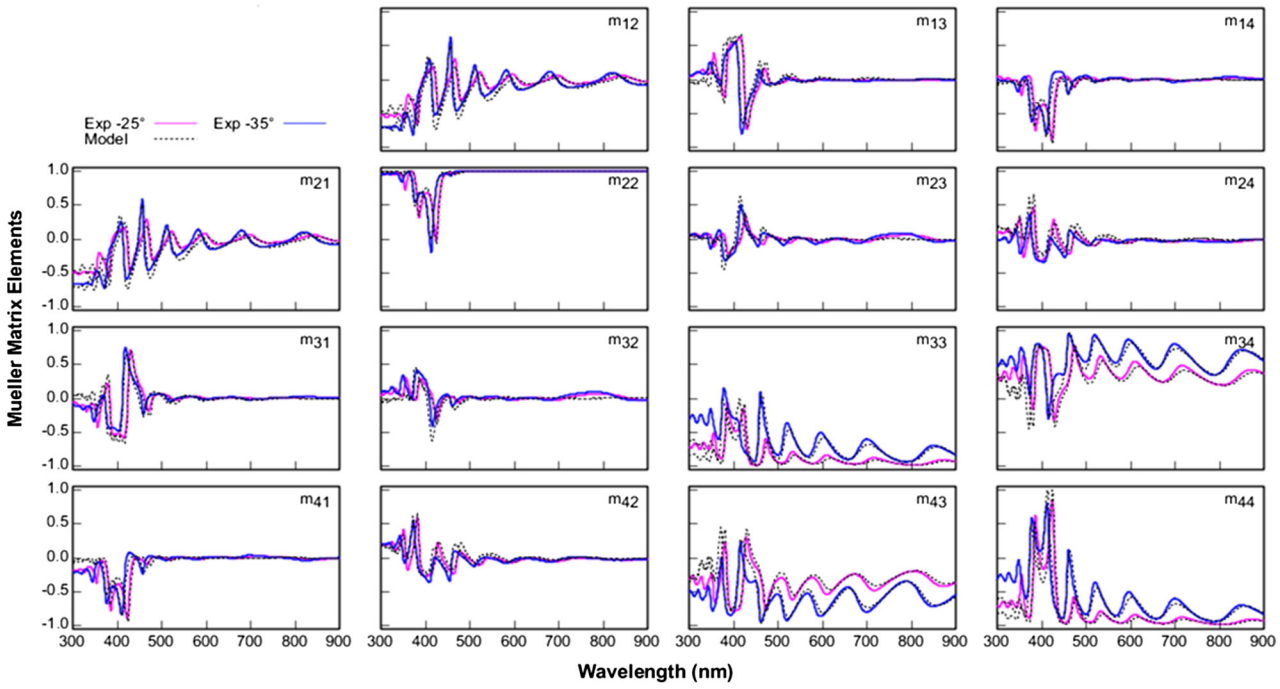
Figs. 5 and 6 show MMSE data in the wavelength region 300–900 nm for a left-handed and a right-handed $Al_{1-x}In_xN$ nanostructured film, respectively. The observed values of m_{41} indicate high degree of circular polarization in the specularly reflected light



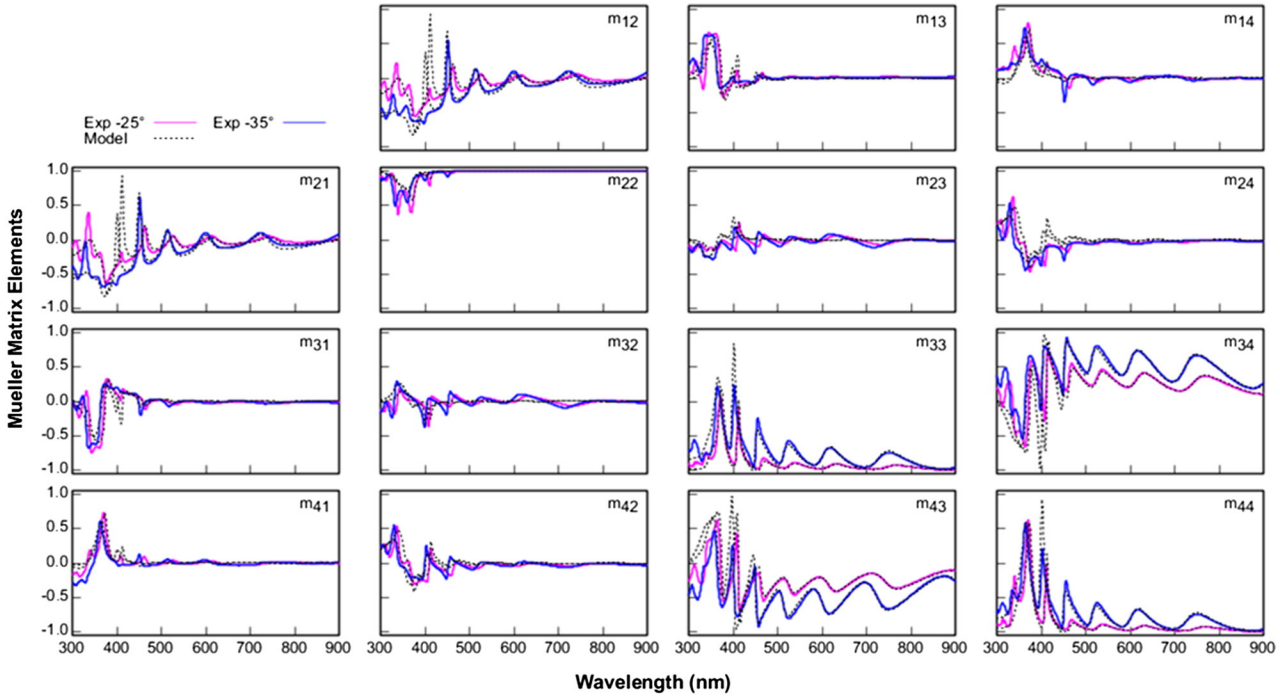
under illumination with unpolarized light. A degree of circular polarization exceeding 0.9 (0.7) is noted in narrow bands at wavelengths close to 423 nm (370 nm) for the left-handed (right-handed) nanostructured film.

Using regression analysis, the optical model described in Section 2 was fitted to the experimental data. The fitting was done in two steps. First the refractive index without dispersion, and the thickness of the layer as well as the surface layer was fitted with a uniaxial Cauchy model in the spectral region 1000–1700 nm. In this region the structural features do not influence the optical response to a significant extent and the films can be considered as uniaxial bulk materials. Experimental data measured at the five incidence angles were fitted simultaneously and a very good fit was achieved. The fit results for a selection of the elements are presented in Fig. 7. The thicknesses obtained for the left-handed sample were 1096 nm for the nanostructured layer and 108 nm for the surface layer. In the second step of the fit the uniaxial model was expanded to a biaxial model. The three directions of the biaxial layer were seeded with the A-values obtained in the first part of the fit, with the in-plane refractive index of the uniaxial model split into two indices in two orthogonal directions in the biaxial model. The thicknesses and the Cauchy parameters A were fixed whereas the dispersion of the refractive indices, as well as the Urbach absorption tails (A_k and B_k) were fitted in all three directions together with φ_0 and T. In this second fit procedure two incidence angles were used to reduce computational time. The lowest angles (25° and 35°) were chosen because they showed the highest values in the off-diagonal Mueller matrix elements and thus carried most information about the optical effects due to the chiral nanostructure. All 72 rotation angles were included in the fit. The model was first employed in a fit to a sample with left-handed spirals. The experimental Mueller matrix of that sample and the best fit can be seen in Fig. 5. Data only in the wavelength range 300–900 nm was included in the fitting process. The lower wavelength limit is due to the fact that the Cauchy model does not work well too close to the band edge of $Al_{1-x}In_xN$. The upper limit is motivated by the fact that the samples were designed to reflect circularly polarized light in the UV–VIS range and the light is only marginally affected by the chirality at longer wavelengths making the part of the spectrum above 900 nm quite featureless. The parameters B in the biaxial film layer were fitted as well as the Urbach absorption tails (A_k and B_k) for three orthogonal directions (x-, y- and z-directions). The resulting real and imaginary parts of the refractive indices for the three different directions of the left handed nanostructured $Al_xIn_{1-x}N$ films can be seen in Fig. 8. The obtained value of T was 4.44. As described in Section 3, the sample underwent five complete turns during deposition. That is, from the fitting the parameter T is slightly lower. This discrepancy is attributed to a delay in the initiation of the chiral nanostructure formation upon start of the deposition and that the tapering of the top part of the nanospirals gives a less pronounced grading of the composition near the surface. The same model approach was used for the sample with right-handed





nanospirals. As above, the thicknesses and the Cauchy parameters *A* of the layers were fitted in the 1000–1700 nm wavelength region, then the dispersion and absorption tail were fitted with fixed thicknesses and *A*-values in the region 300–900 nm. The fit to the experimental data can be seen in Fig. 6. The thickness of the graded layer was in this case 967 nm and the interface layer 77 nm. The obtained value for *T* was −4.56 where the minus sign indicates that the rotation is in the opposite direction compared to the left-handed case. The model-fitted structural properties of the two samples are summarized in Table 1. The corresponding findings of



Please cite this article as: R. Magnusson, et al., Thin Solid Films (2014), http://dx.doi.org/10.1016/j.tsf.2014.02.015

ARTICLE IN PRESS

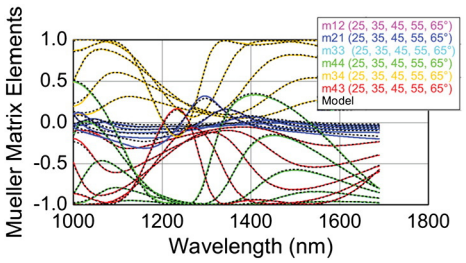
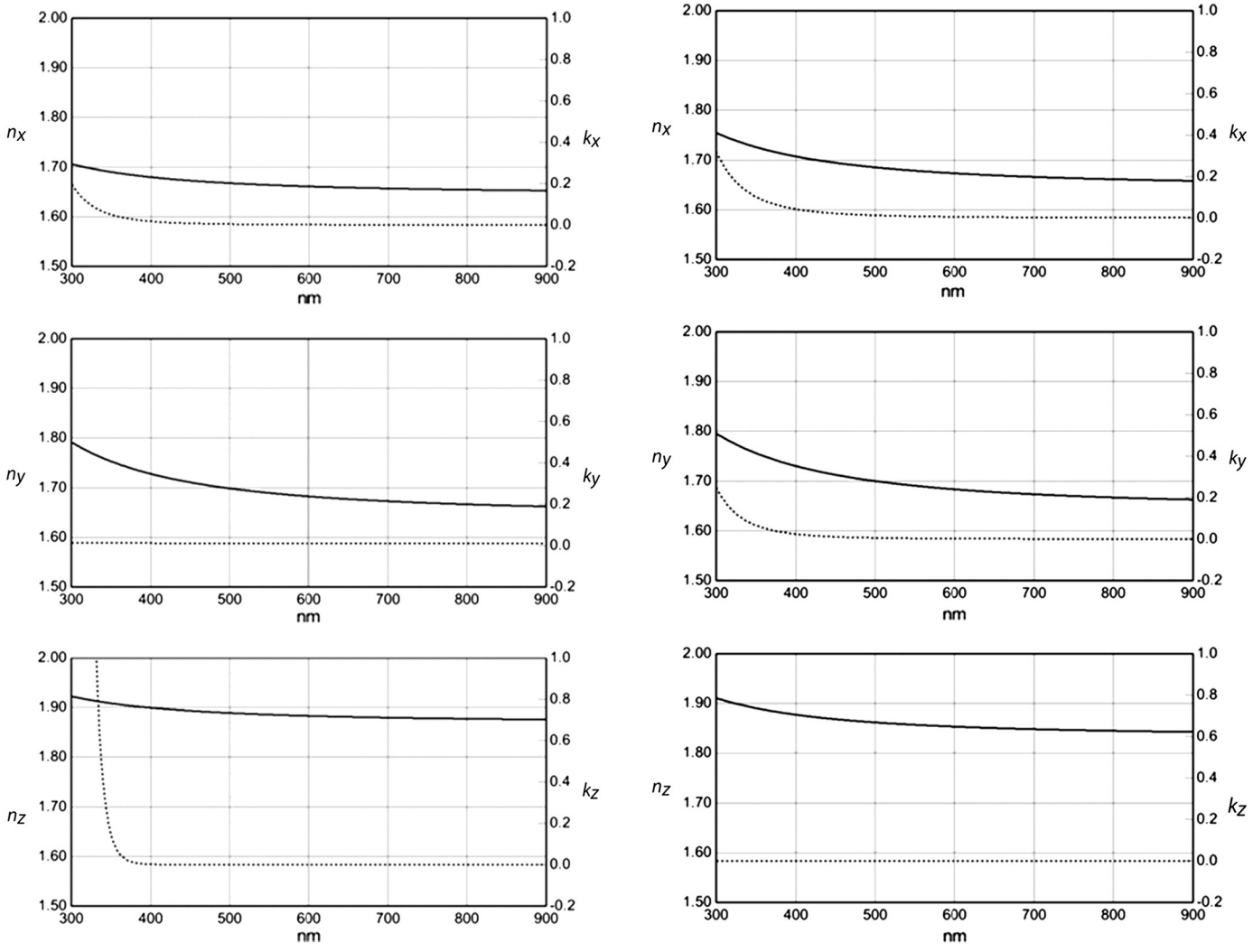


Table 1
Structural properties of the chiral nanostructure.

	Left-handed spirals	Right-handed spirals
Thickness of film layer	1096 nm	967 nm
Thickness of surface layer	108 nm	77 nm
Number of turns, T	4.44	−4.56

the optical properties for the right-handed chiral film are found in Fig. 9. In general the optical properties are consistent with previous work [9] considering the amount of In content and the structural properties. The differences in optical properties between left- and right-handed films may depend on variations in composition, in the lateral gradient or in the porosity of the film. The model we have used does not take the external chirality into account, only the internal. If the external chirality would have been included, a second Euler angle θ, should have a non-zero value. During our modeling we have found, however, that including θ does not increase the goodness of the fit and have therefore decided to leave it out of the model.

In summary we conclude that the CLEG method can be used to produce interesting nanostructured films with left- as well as right-handed chirality. Both films have narrow bands reflecting light with high degree of left- and right-circular polarization, respectively, originating from a compositional gradient within the nanocolumns. Many factors make these structures very complex. Still, we were able to obtain acceptable model fits to the MMSE-data and extract structural and optical information.



Please cite this article as: R. Magnusson, et al., Thin Solid Films (2014), http://dx.doi.org/10.1016/j.tsf.2014.02.015

ARTICLE IN PRESS

Acknowledgments

The authors would like to acknowledge the Knut and Alice Wallenberg Foundation and the Swedish Research Council for financial support.

References

[1] J.K. Gansel, M. Thiel, M.S. Rill, M. Decker, K. Bade, V. Saile, G. von Freymann, S. Linden, M. Wegener, Science 325 (2009) 1513.
[2] K.M. Krause, M.J. Brett, Adv. Funct. Mater. 18 (2008) 3111.
[3] Y. Zhou, K.-M. Chen, Y. Huang, S.-T. Wu, The 20th Annual Meeting of the IEEE Lasers and Electro-Optics Society, LEOS, 2007, p. 210.
[4] N. Gupta, D. Suhre, Appl. Opt. 46 (2007) 2632.
[5] C.-L. Hsiao, R. Magnusson, J. Palisaitis, P. Sandström, P.O.Å. Persson, S. Valyukh, L. Hultman, K. Järrendahl, J. Birch, Curved-lattice epitaxial growth of $Al_xIn_{1-x}N$ nanospirals with tailored chirality, 2014. (submitted for publication).
[6] G.Z. Radnóczi, T. Seppänen, B. Pécz, L. Hultman, J. Birch, Phys. Status Solidi (A) 202 (2005) R76.
[7] C.L. Hsiao, J. Palisaitis, M. Junaid, P.O.A. Persson, J. Jensen, P. Sandstrom, Q.X. Zhao, L. Hultman, L.C. Chen, K.H. Chen, J. Birch, Thin Solid Films 524 (2012) 113.
[8] M. Bass, V.N. Mahajan, E.W. Van Stryland, G. Li, C.A. MacDonald, C. DeCusatis, Optical Society of America, Handbook of Optics, , McGraw-Hill, New York, 2010.
[9] E. Sakalauskas, H. Behmenburg, C. Hums, P. Schley, G. Rossbach, C. Giesen, M. Heuken, H. Kalisch, R.H. Jansen, J. Bläsing, A. Dadgar, A. Krost, R. Goldhahn, J. Phys. D. Appl. Phys. 43 (2010) 365102.
[10] H. Fujiwara, Spectroscopic Ellipsometry: Principles and Applications, , Wiley, West Sussex, 2007..

Please cite this article as: R. Magnusson, et al., Thin Solid Films (2014), http://dx.doi.org/10.1016/j.tsf.2014.02.015